

Article

Understanding Temporal Patterns and Determinants of Ground-Level Ozone

Junshun Wang¹, Jin Dong¹, Jingxian Guo¹, Panli Cai¹, Runkui Li^{1,2,3,4,*} , Xiaoping Zhang¹ , Qun Xu^{5,6} and Xianfeng Song^{1,3} 

- ¹ College of Resources and Environment, University of Chinese Academy of Sciences, Beijing 100049, China
² Binzhou Institute of Technology, Binzhou 256606, China
³ State Key Laboratory of Resources and Environmental Information System, Institute of Geographic Sciences and Natural Resources Research, Chinese Academy of Sciences, Beijing 100101, China
⁴ Beijing Yanshan Earth Critical Zone National Research Station, University of Chinese Academy of Sciences, Beijing 101408, China
⁵ Department of Epidemiology and Biostatistics, Institute of Basic Medical Sciences Chinese Academy of Medical Sciences, School of Basic Medicine, Peking Union Medical College, Beijing 100005, China
⁶ Center of Environmental and Health Sciences, Chinese Academy of Medical Sciences, Peking Union Medical College, Beijing 100005, China
* Correspondence: lirk@ucas.ac.cn; Tel.: +86-10-69672954

Abstract: Ground-level ozone pollution causes adverse health effects, and the detailed influences of meteorological factors and precursors on ozone at an hourly scale need to be further understood. We conducted an in-depth analysis of the phase relationships and periods of ground-level ozone in Shunyi station, Beijing, and contributing factors using wavelet analysis and geographic detectors in 2019. The combined effects of different factors on ozone were also calculated. We found that temperature had the strongest influence on ozone, and they were in phase over time. NO₂ had the greatest explanatory power for the temporal variations in ozone among precursors. The wavelet power spectrum indicated that ozone had a periodic effect on multiple time scales, the most significant being the 22–26 h period. The wavelet coherence spectrum showed that in January–March and October–December, NO₂ and ozone had an antiphase relationship, largely complementary to the in-phase relationship of temperature and ozone. Thus, the main influencing factors varied during the year. The interactions of temperature with NO₂ significantly affected the temporal variations in ozone, and explanatory power surpassed 70%. The findings can deepen understanding of the effects of meteorological factors and precursors on ozone and provide suggestions for mitigating ozone pollution.

Keywords: ozone; meteorological factor; temporal variation; wavelet analysis; geographic detector



Citation: Wang, J.; Dong, J.; Guo, J.; Cai, P.; Li, R.; Zhang, X.; Xu, Q.; Song, X. Understanding Temporal Patterns and Determinants of Ground-Level Ozone. *Atmosphere* **2023**, *14*, 604. <https://doi.org/10.3390/atmos14030604>

Academic Editors: Guiqian Tang, Dongsheng Ji and Xiaolan Li

Received: 25 February 2023

Revised: 18 March 2023

Accepted: 21 March 2023

Published: 22 March 2023



Copyright: © 2023 by the authors. Licensee MDPI, Basel, Switzerland. This article is an open access article distributed under the terms and conditions of the Creative Commons Attribution (CC BY) license (<https://creativecommons.org/licenses/by/4.0/>).

1. Introduction

The atmospheric environment is profoundly affected by intense human activities and extreme weather, and air pollution has become a major environmental concern in many countries [1,2]. China, the largest developing country, has implemented a series of much stricter air pollution control measures since the last decade, sacrificing rapid economic growth to control air pollution [3–7]. Although monitoring data have demonstrated that the concentrations of many pollutants (e.g., SO₂ and PM_{2.5}) have decreased dramatically in China in recent years, ozone (O₃) concentrations have exhibited an opposite and increasing trend. Ozone can irritate the respiratory tract and impede blood oxygenation, leading to potential systemic effects when the tropospheric concentration exceeds a certain threshold [8,9]. Under such context, deeper understandings of the temporal trends of ozone concentrations and the complex underlying influencing factors are needed for targeted air pollution control [10].

The formation and elimination processes of ozone are complicated. Human activities do not emit ozone directly, but transportation, thermal power generation, and the petrochemical industry emit considerable amounts of ozone precursors (e.g., NO_x and VOCs) [11]. Ozone is formed when heat and sunlight cause chemical reactions between these precursors [12]. Thus, the precursors and meteorological conditions are both important for ozone concentration. Previous studies have demonstrated the significant effects of various meteorological factors on ozone, such as temperature [13,14], humidity [15], air pressure [16], wind direction [14], and wind speed [17]. Meteorological factors and ozone concentrations oscillate sharply within a day or days and also fluctuate remarkably by season [18–20].

Due to the high complexity of ozone, revealing its temporal patterns and relating factors is a challenge. Although there have been several studies investigating the drivers of ozone concentrations, the knowledge of ozone, such as periodicity and the joint effects of the various influencing factors, remains lacking. First, previous studies have mostly focused on large areas, such as countries [21–23], urban agglomerations [24,25], and cities [26]. These studies often used the mean or other integrated values to characterize the ozone concentrations in a certain region with sparse monitoring stations. However, ozone concentration can be extremely heterogeneous across regions, even over short distances. Such large-scale approaches aggregate the spatial and temporal variability and can hardly obtain the specific relationships between ozone and its influencing factors. Using time series data from the same station can avoid the influences of complex spatial factors and obtain a more accurate and detailed relationship. Second, most studies have focused on the spatial variability of ozone [27], but inadequate attention has been paid to its temporal features and causes, which are critical to explore the ozone formation process and control ozone pollution. Third, many studies have focused on the analysis of annual and monthly variability of ozone and its influencing factors, while ozone concentrations and meteorological factors can vary dramatically on an hourly scale [28,29]. Short-term changes in ozone are also important to reveal its detailed processes and causes. The long-term studies cannot highlight the precise relationships on an hourly scale.

Notably, an increasing number of scholars have used more advanced models to quantify the impact of various meteorological factors on surface ozone concentrations, such as quantile and multiple linear regression models [22,30–33]. These models, while focusing on the goodness of model fit, are limited in quantifying the effect of each individual factor and the interactions among factors. Because of the complexity of ozone formation [34,35] and the strong oscillations and periodicity of the meteorological factors and ozone precursors at an hourly scale [36], it is difficult to reveal the complete temporal patterns of ozone. At present, few studies have analyzed the effects of the influencing factors on the periodicity, phase relationship, correlation, or differentiation of ozone distribution at hourly scales. Such information is critical for exploring the effects of meteorological factors and anthropogenic precursors on ground-level ozone concentrations in detail. However, wavelet analysis and geodetectors can well make up for the shortcomings of the above methods. Wavelet analysis is a method of representing signals with a finite-length or fast-decaying “mother wavelet”, and the signals are usually time series. Wavelet analysis can quickly extract the variation characteristics of time series such as periodicity. Moreover, the wavelet coherence spectrum can reflect both the correlation and time lag between variables, which overcomes the shortcoming of the traditional correlation analysis methods (such as Pearson, Spearman, and Kendall) [13]. Due to its ability to extract hidden features, wavelet analysis has been widely used in the study of many atmospheric pollutants [37–40]. “Geodetectors” is an effective method for exploring the hierarchical heterogeneity in geography [41–45]. Geodetectors include factor detector and interactive detector, which are used to detect the drivers of a single factor and factor interaction on the dependent variable, respectively. Geodetectors are often used to analyze the heterogeneity of spatial distribution, but it still has superior performance in calculating temporal heterogeneity,

especially quantitatively calculating joint effects of different factors, which is difficult to express in traditional models.

To fill the knowledge gap in this area, this study aims to explore the following two issues: (a) using wavelet analysis to investigate the variation character and periodic oscillation properties of ozone on an hourly scale in the time–frequency domain and explore the correlation and phase relationship between the influencing factors and ozone; and (b) quantitatively estimate the explanatory power of each factor and their joint effects on ground ozone concentration. Based on the ozone-influencing-factor relationships and phase relationship analysis, a more comprehensive understanding of ozone temporal variation will be achieved, which is the basis to support practical suggestions for ozone pollution prediction and control.

2. Materials and Methods

2.1. Data Sources

According to related studies [22,46,47], there are several major determinants of ozone, including reactants, reaction conditions, regional transportation, and seasonal effects. To describe the detailed ambient conditions of ozone, we selected eight meteorological factors, including temperature, dewpoint temperature, wind speed (including U and V components), surface net solar radiation, surface air pressure, solar altitude, and relative humidity, as the influencing factors [48]. NO₂ was selected as the anthropogenic precursor of ozone. Although VOCs are important for short-term ozone generation, the hourly monitoring cost of VOCs is too high, and there are no available VOCs data to access for this study. Furthermore, VOCs include a variety of compounds, and different compounds have different contributions to the generation of ozone, which adds extra complexity. Therefore, this study did not include VOCs as precursors of ozone during analysis. The theoretical relationships between the influencing factors and selected proxy variables are presented in Figure 1. The detailed parameters from ERA5 land reanalysis data and observation stations are listed in Table S1.

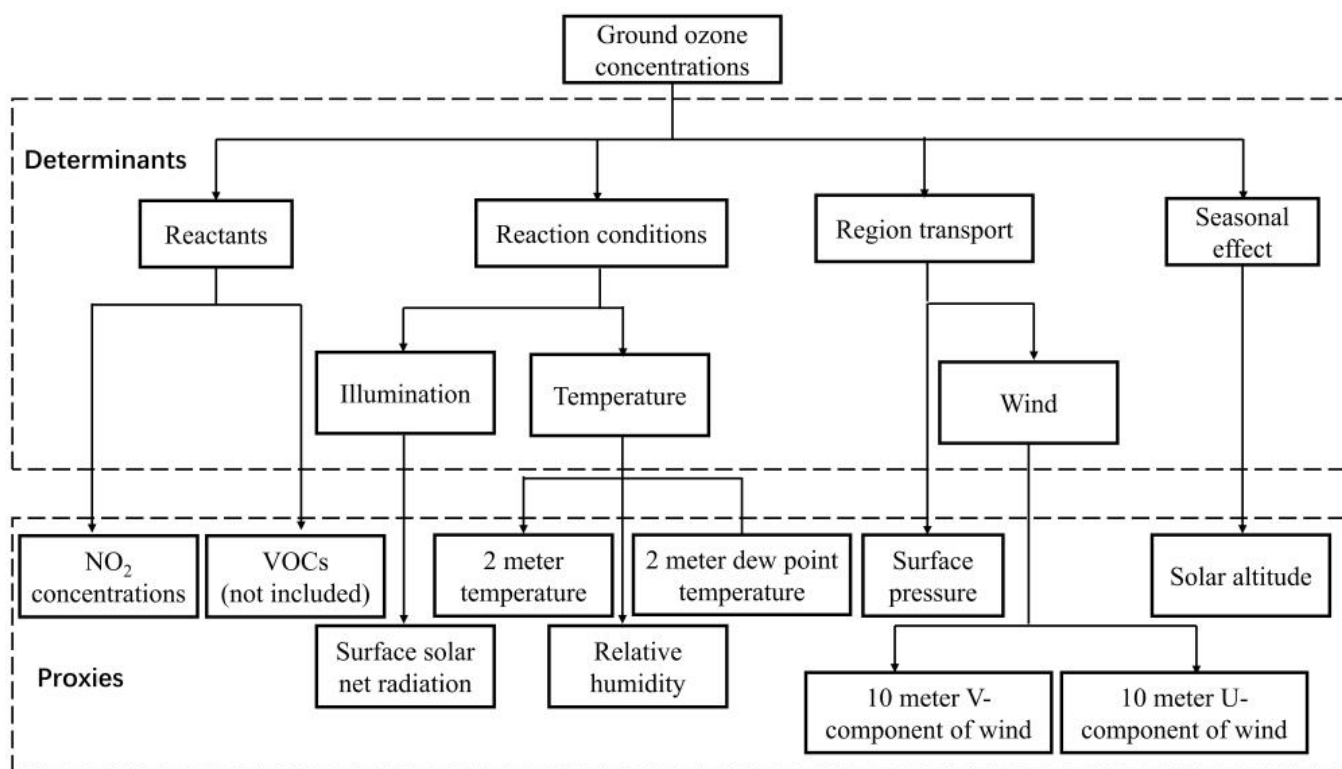


Figure 1. Ozone concentration determinants and their proxies.

2.1.1. Ground Ozone and Its Precursors

Ground-level ozone and NO₂ concentrations were obtained from the monitoring stations of the National Environmental Monitoring Center of China (<http://www.cnemc.cn/> (accessed on 15 July 2021)). Considering fewer missing data and higher representativeness of the geographical environment where the station is located, Shunyi station (40.1269° N, 116.655° E), in the northeast of Beijing, was chosen for this study. Hourly observations from 1 January at 15:00 to 31 December at 23:00 in 2019 were collected and prepared. The total number of observations was 8745, with 447 missing data values due to equipment or network errors, which accounted for 5.12%. To fill in the missing values, we attempted linear interpolation, quadratic curve interpolation, polynomial interpolation, and spline function interpolation for the whole dataset. However, none of these methods was found to fill the missing data well. Finally, we calculated the number and percentage of missing gaps for variables (Table S2), set 5 h as the threshold of time span, and conducted linear interpolation to fill in the missing values if the continuous missing values were less than 5. Otherwise, if there were more than five continuous missing values, the mean value for the same hour from the previous three days and the following three days was used. After the above data preparation process, the filled results were found to better reflect the periodicity of ozone concentrations from the perspective of time series and exhibited a reasonable oscillation amplitude. For NO₂, the missing values were filled in the same way as for ozone.

2.1.2. ERA5 Land Meteorological Data

Ground meteorological monitoring stations are rarely located in the same position as air pollution monitoring stations, and only limited meteorological parameters are provided. Therefore, full-coverage meteorological reanalysis data were used to derive the required meteorological parameters. The meteorological data in this study were extracted from the ERA5 Land dataset (<https://www.ecmwf.int/en/forecasts/datasets/reanalysis-datasets/era5> (accessed on 18 July 2021)). ERA5 Land is a reanalysis dataset, which combines model data with worldwide observations into a complete and consistent global dataset [49]. We extracted and calculated the time series data of ERA5 Land for the location of the air pollution monitoring site. The meteorological parameters included 2 m temperature, 2 m dewpoint temperature (2 m temperature), 10 m U component of wind (10 m U wind), 10 m V component of wind (10 m V wind), surface pressure, surface net solar radiation (SNSR), relative humidity (RHU), and solar altitude data. Specifically, the 2 m temperature and 2 m dewpoint temperature represent the values at 2 m above the ground surface. The 10 m U component of the wind represents the east–west component of the horizontal wind at 10 m above the ground surface, with positive values indicating from west to east. Similarly, the 10 m V component of the wind is the north–south component of the horizontal wind. Because the densely populated area of Beijing is mainly to the south of the monitoring point, the influence of wind direction was also considered.

2.2. Methods

2.2.1. Continuous Wavelets, Cross Wavelets, and Wavelet Coherence

- Continuous wavelet transform

Wavelet analysis is an effective tool for periodic and unstable O₃ and meteorological factors. However, few studies have conducted a wavelet analysis to explore the features over time. Wavelet analyses compensate for the traditional Fourier transform, which can only display frequency domain information and the uncertainty of the window selection of the short-term Fourier transform [50]. Wavelet analyses can reflect local variation characteristics along the time series and perform a multiscale detailed analysis of the signal. The Morlet wavelet is a plural form wavelet, and its real and imaginary parts differ by $\pi/2$, which eliminates the oscillation of the real wavelet transform coefficient modulus [51]. To

ensure a better balance between time and frequency localization analysis [52], the following Morlet wavelet was used for analysis:

$$\Psi_0(t) = \pi^{-\frac{1}{4}} e^{i\omega_0 t} e^{-\frac{t^2}{2}} \tag{1}$$

where ω_0 is the dimensionless frequency, t is the dimensionless time, and i represents the imaginary unit. When $\omega_0 = 6$, the wavelet scale s is approximately equal to the Fourier period. The continuous wavelet transform can be expressed as follows:

$$W_n(s) = \sum_{k=0}^{N-1} \hat{x}_k \hat{\Psi} \times (s\omega_k) e^{i\omega n \delta t} \tag{2}$$

The continuous wavelet transform can be used to analyze the periodicity and oscillation characteristics of a single factor in the time series, but an analysis of the correlation and causality between ozone and its influencing factors requires the use of cross wavelet and wavelet coherence.

- Cross wavelet

Through a time–frequency analysis of multiple time scales, the relationship between two time series (O_3 and its influencing factors) can be determined. With $W_n^X(s)$ and $W_n^Y(s)$ as the continuous wavelet transform results of X_n and Y_n , respectively, the cross wavelet transform (XWT) can be defined as

$$W_n^{XY}(s) = W_n^X(s) W_n^{Y*}(s) \tag{3}$$

$W_n^{Y*}(s)$ is the complex conjugate of $W_n^Y(s)$, and the power of the crossed wavelet is defined as $|W_n^{XY}(s)|$, reflecting the resonance energy of two time series in the time–frequency domain. The larger the power, the higher the correlation between two time series [53]. The significance of the XWT power spectrum is to compare it with the red noise standard spectrum. Assuming that the expected spectra of the two time series X and Y are red noise spectra P_k^X and P_k^Y , the crossed wavelet power spectrum distribution has the following relationship:

$$D \left(\left| \frac{|W_n^X(s)| |W_n^{X*}(s)|}{\delta_X \delta_Y} \right| < p \right) = \frac{Z_\nu(p)}{\nu} \sqrt{P_k^X P_k^Y} \tag{4}$$

$Z_\nu(p)$ is the confidence level related to probability P of the probability density function (PDF), which is defined by the square root of the product of the two χ^2 distributions, and ν is the degree of freedom. When $\nu = 2$ and the significance level is set at $\alpha = 0.05$, Z_2 (95%) equals 3.999. If the time series X and Y satisfy the significance test, they will be considered significantly correlated under the red noise test.

- Wavelet coherence

The power spectrum of the cross wavelet can only reveal whether two time series have a common high-energy region, whereas the wavelet coherence spectrum can be used to measure the local correlation degree of two time series, similar to the piecewise correlation coefficient. Even if the two series are in the low-energy region, their correlation may be significant. Therefore, the significant area of the wavelet coherence spectrum is generally larger than that of the cross wavelet spectrum [52]. The wavelet coherence spectra of the two time series X and Y are defined as

$$R_n^2(s) = \frac{|S(s^{-1} W_n^{XY}(s))|^2}{S(s^{-1} |W_n^X(s)|^2) S(s^{-1} |W_n^Y(s)|^2)} \tag{5}$$

S is a smoother, defined as

$$S(W) = S_{scale}(S_{time}(W_n(s))) \tag{6}$$

S_{scale} is the smoothing parameter of the wavelet-scale coordinate axis, and S_{time} is the smoothing parameter of the time axis. For the Morlet wavelet used in this study, a suitable smoother is defined as follows:

$$S_{time}(W)|_s = \left(W_n(s) \times c_1^{\frac{-t^2}{2s^2}} \right) |_s \tag{7}$$

$$S_{time}(W)|_s = \left(W_n(s) \times c_2 \prod(0.6s) \right) |_s \tag{8}$$

C_1 and C_2 are standardization constants, Π represents the rectangular function, and coefficient 0.6 is the empirical scale of the Morlet wavelet. The Monte Carlo approach has also been used to evaluate the significance of the wavelet coherence spectrum [52]. The average angle of the phase difference arrow and 95% confidence interval are used for the wavelet coherence spectrum, and only the phase difference arrow with $R_n^2(s) \geq 0.5$ is given in the results.

2.2.2. Geodetectors

Considering the significant seasonality of ozone, the correlation between ozone and its influencing factors may also vary with season. To investigate this temporally nonstationary relationship, we stratified the factors from a temporal perspective with natural breakpoints after stratification by season, and then detected factors and their interactions using geodetectors [54]. A geographic detector was originally used to detect spatially stratified heterogeneity. However, the concept of “stratification” is not limited to geospace, and the stratification of variables can be spatial, temporal, or by attribute [55]. The core assumption of geodetectors is that if an independent variable has a significant influence on a dependent variable, the distributions of the two variables should be similar. Here, we extend the concept of “stratification” to the time series of ozone and the related factors to explore the temporal relationships among variables.

- Factor detector

To detect the explanatory power of factor X to Y , the value q can be calculated as follows:

$$q = 1 - \frac{\sum_{h=1}^L N_h \delta_h^2}{N \delta^2} = 1 - \frac{SSW}{SST} \tag{9}$$

$$SSW = \sum_{h=1}^L N_h \delta_h^2 \tag{10}$$

$$SST = N \delta^2 \tag{11}$$

$h = 1, 2, \dots, L$ is the stratum of variable X ; N_h and N are the number of units in stratum h and in all strata, respectively; and δ_h^2 and δ^2 represent the variance of stratum h and the global total variance, respectively. The larger the value of q , the stronger the decisive power of the independent variable X on the distribution of the dependent variable Y , and vice versa. After a simple transformation of the q value, it satisfies the noncentral F distribution, and its significance can be assessed [54].

- Interactive detector

Single-factor detection cannot be used to explore the joint effects of factors on ozone. It is difficult to detect the joint effect of factors on the enhancement or weakening of ozone pollution using traditional methods that cannot exclude the effect of multicollinearity [27]. However, the interactive detector can efficiently calculate the joint effects of the two factors on ground-level ozone concentration. In this study, the interactive detector first calculates

the q values of $X1$ and $X2$ separately to derive $q(X1)$ and $q(X2)$ and then calculates the interaction of the two variables $q(X1 \cap X2)$. These three powers are compared to determine whether the interaction enhanced or weakened the explanatory power of the ozone concentration level.

3. Results and Discussion

3.1. Time–Frequency Characteristics of O_3 and Its Influencing Factors

The preliminary data exploration revealed that O_3 and its influencing factors have clear seasonality, which can also be confirmed by the wavelet transform. The year is divided into spring (March to May), summer (June to August), autumn (September to November), and winter (December to February) according to the meteorological features and customs rules of China.

From the time–frequency domain, the ground-level ozone concentration variation is characterized by instability and periodicity. Figure 2b shows that the wavelet power spectrum of ozone has a distinct 22–26 h period band from March to November, which indicates that there is a significant daily periodic signal of ozone concentrations at the 22–26 h time scale. This result quantitatively confirms the day-cycle characteristics of ozone.

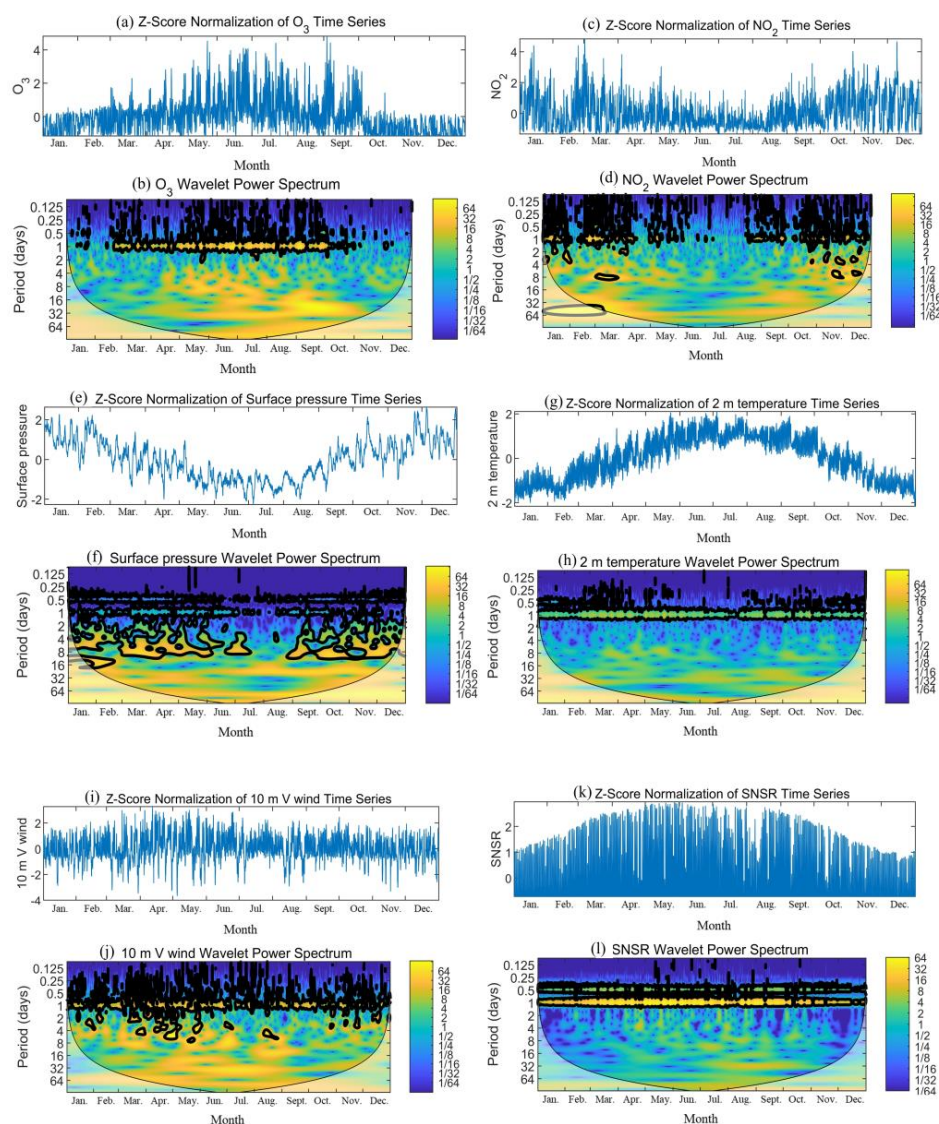


Figure 2. Z-score normalization time series and wavelet power spectrum for (a,b) O_3 ; (c,d) NO_2 ; (e,f) surface pressure; (g,h) 2 m temperature; (i,j) 10 m V wind; and (k,l) net surface net solar radiation.

Furthermore, we performed a Morlet wavelet analysis on all the factors. Several influencing factors exhibit similar periodic characteristics to ozone, such as the 2 m temperature (Figure 2h). However, the time–frequency distribution patterns of some factors are different from ozone. For example, NO₂ does not exhibit a 24 h cycle in summer (June–August). In contrast, NO₂ in winter shows a distinct 24 h scale cycle when ozone periodicity is not significant (December–February), and the concentration of NO₂ is lower in summer and higher in winter, which demonstrates an opposite trend to that of ozone across the year (Figure 2c). Surface pressure has a stronger 4–8 day cycle in the months of the year except July and August (Figure 2f). The 10 m V component of the wind has a relatively continuous 24 h scale period in the annual time distribution (Figure 2j). The net surface solar radiation is considerably higher in summer and lower in winter, which is caused by the revolution of the Earth and the incidence angle of sunlight. Notably, in Figure 2l, the net surface solar radiation has two significant periods, corresponding to 1 d and 0.5 d, respectively. This also explains the fragmentary periodic signal of ozone on an hourly scale. The wavelet power spectra of the other factors are provided in Figures S1–S4.

The line charts represent the Z-score normalization time series for each factor, which are the results of normalizing the original data with 0 as the mean and one unit as one standard deviation. In the wavelet power spectrum, the left and right axes represent the period and periodic intensity, respectively, and the bottom axis is time. The yellow represents a higher periodic intensity and the blue represents a lower periodic intensity. The thick contour encloses regions of greater than 95% confidence for a red noise process, and the thick curve is the cone of influence (COI).

3.2. Correlation among Influencing Factors and Ozone

Traditional methods cannot obtain the phase relationship of the periodic sequence, whereas cross wavelets and wavelet coherence can effectively diagnose the correlation and time lag between different signals, highlight the common energy region in the time–frequency domain between ozone and its impact factors, and reveal the causal relationship between them [52]. To comprehensively analyze the influencing factors that affect ground ozone concentrations, 10 independent variables, including the precursors and meteorological factors, were selected for cross wavelet and wavelet coherence analyses. Based on related studies [56–60], the precursor NO₂ and meteorological factor 2 m temperature were explained in detail, and the results for other factors are provided in Figures S6–S18. The key phase relationships and periods between the other factors and ozone are summarized in Table S3.

Figure 3a shows the crossed spectrum of ozone and NO₂. The high-energy area of the wavelet is mainly concentrated in the period of 22–26 h. Although there is a short break from mid-January to mid-February, the relationship between NO₂ and ozone during the 22–26 h period in 2019 is significant in general. In Figure 3b, on the 0.25–8 d scale, NO₂ and O₃ are in an antiphase, and this relationship almost lasts for the entire study period (except from May to September). For the phase difference, the NO₂ and O₃ concentrations change in opposite directions at multiple scales. NO₂ produces nitric oxide (NO) via photolysis, which then consumes ozone through titration. In the complex reaction process, concentrations of NO₂ that are either too high or too low suppress ozone concentrations, which is also supported by the Empirical Kinetic Modeling Approach (EKMA) curve proposed by the United States Environment Protection Agency (USEPA) [61]. From the specific analysis results, in January–May and October–December, NO₂ and O₃ are in a significant antiphase at several time scales. In mid-August–November, in addition to the 22–26 h period scale, there are correlations on the 10–15 d and 20–30 d scales, but the phase angle arrow faces downward, indicating that NO₂ lags the O₃ changes on a larger time scale in autumn.

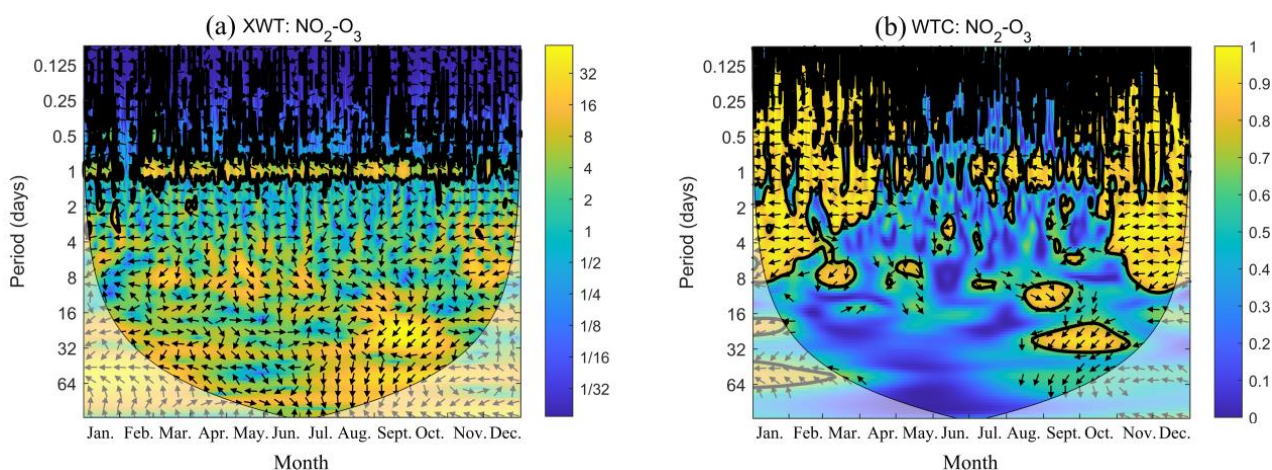


Figure 3. (a) Cross wavelet spectrum (XWT); (b) wavelet coherence spectrum (WTC) of NO₂ and O₃.

The left axis represents the period, the right axis represents the intensity of the common period in the XWT and the consistency of the changing trends in the WTC, and the bottom axis represents time. The yellow represents a larger correlation coefficient and blue represents a smaller correlation coefficient. The area surrounded by the thick black solid line indicates the area that passes the 95% red noise confidence test, and the black solid line envelope is the conical influence domain; the relative phase relationship is indicated by the arrows (in phase points to the right, antiphase points to the left, NO₂ leads O₃ 1/4 period when pointing straight up).

As indicated in Figure 4, temperature and O₃ have the most significant resonant cycles on the 22–26 h scale in the positive phase in 2019, indicating that there is a significant correlation between the two on an hourly scale. This also suggests that ozone and temperature change simultaneously. Higher temperatures can provide energy for the movement of atoms and molecules and accelerate the molecular decomposition of the reaction process, thereby accelerating ozone production [62]. Furthermore, temperature increases with the solar radiation from sunlight, which is a significant factor in the overall O₃ generation reaction. Figure 4b demonstrates that there is also a good correlation between the air temperature and ground-level ozone concentrations on the 20–30 d cycle scale from May to November, with a difference of approximately 360° in direction (arrow level to the right). The correlation was significant ($\alpha = 0.05$) in the standard spectrum test for red noise. There was also a significantly positive correlation for 6–10 d during March–August, indicating a multiscale effect of temperature on ozone generation.

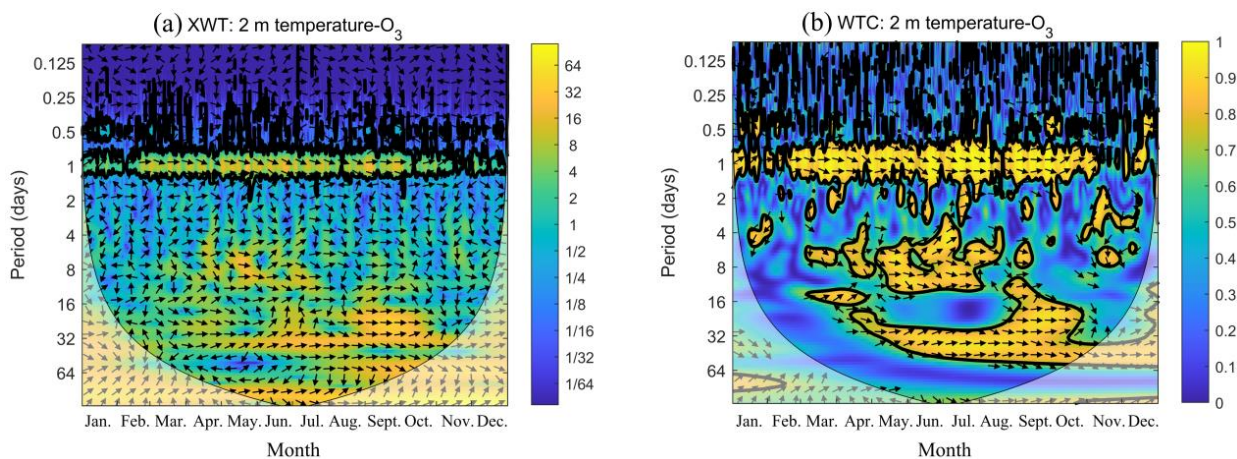


Figure 4. (a) Cross wavelet spectrum (XWT); (b) wavelet coherence spectrum (WTC) of 2 m temperature and O₃.

The left axis represents the period, the right axis represents the intensity of the common period in the XWT and the consistency of the changing trends in the WTC, and the bottom axis represents time. The yellow represents a larger correlation coefficient and blue represents a smaller correlation coefficient. The area surrounded by the thick black solid line indicates the area that passes the 95% red noise confidence test, and the black solid line envelope is the conical influence domain; the relative phase relationship is indicated by the arrows (in phase points to the right, antiphase points to the left, temperature leads O₃ 1/4 period when pointing straight up).

3.3. Stratified Heterogeneity of Ozone and Detection of Factor Effects

To quantitatively evaluate the effects of the precursors and meteorological factors on ground-level ozone concentrations, all factors were stratified after considering the seasonality factors. The results of the factor detection indicate that O₃ had significant heterogeneity in the time series distribution, and all 10 factors have significant effects on the temporal heterogeneity of ozone concentrations, but the strength of the effects varied substantially (Table 1). It can be found that the value of *q* is between 0.22 and 0.64, and all have passed the significance test, indicating that the factors used in the study have 22% to 64% explanatory power on the time distribution of ozone during the study period. Among the meteorological factors, temperature and net surface radiation have the highest explanatory power for ground-level ozone concentrations; in particular, temperature explained 64% of the ozone variation. Although ambient temperature typically correlates positively with solar radiation, it has its own special contribution to ozone generation in many ways. High temperature causes high NO_x emissions from soil and biogenic VOCs which are important precursors of ozone. PAN is generated through the oxidation of acetaldehyde in the presence of NO_x in a hydrocarbon-rich environment. The formation of PAN serves as sinks for both NO_x and peroxy radicals, which can reduce the reactants for the ozone generation [63,64]. Moreover, dry deposition to vegetation is an important sink of tropospheric ozone, while high temperature would suppress stomatal uptake and decrease dry deposition [65]. Regarding the net surface solar radiation, the ERA5 reanalysis dataset during night-time hours shows zero solar radiation. However, ozone transport still occurs at night. Therefore, the temporal divergence explanatory power of the net surface solar radiation did not reach the expected value, with 0.36 in this study. The decisive power of NO₂ on ozone concentration is 41% [66]. The effect of NO₂ concentration on O₃ production is complex. NO₂ acts as a reactant for O₃ production, and sufficient NO₂ facilitates ozone production, but too much NO₂ inhibits O₃ concentrations [67]. Therefore, the power derived above is reasonable.

Table 1. Statistics of impact factor detection by geodetectors for ozone concentrations.

Index	2 m Temperature	10 m U-Wind Component	10 m V-Wind Component	Net Surface solar Radiation	Surface Pressure	2 m Dewpoint Temperature	RHU *	Solar Altitude	NO ₂
q statistic	0.64	0.22	0.23	0.36	0.27	0.25	0.22	0.29	0.41
p value	<0.001	<0.001	<0.001	<0.001	<0.001	<0.001	<0.001	<0.001	<0.001

* Relative humidity: RHU.

The interaction between the factors is common, which is also in line with reality. Because the geodetectors are calculated using the ratio of total intra-stratum variance to global variance, it ingeniously avoids the covariance problem of traditional methods. The *q* values of each pair of factors indicate that the joint effects of the factors on ozone concentrations are all enhancing effects (Table 2). Among them, the interaction of temperature and NO₂ have an explanatory power of 74% for the temporal variations in ozone concentrations, which is extremely significant. This can be attributed to the fact that both are direct factors associated with the ozone production reaction. Temperature can accelerate the ozone production reaction and affect the transport of atmospheric pollutants by influencing other factors, such as relative humidity and wind. While NO₂ is an ozone precursor, higher temperatures

can accelerate its decomposition speed; therefore, the joint effect of temperature and NO₂ is crucial for ozone concentrations. In addition, the interaction of net surface radiation and the north–south component of wind has 44% explanatory power on the variation in ozone concentrations. Because the net surface solar radiation characterizes the intensity of input energy, and sunlight is an essential condition for ozone production, this factor should have explanatory power for the variation in ozone concentrations. Regional transport influences ozone concentrations, which is revealed by the 10 m V-wind component and 10 m U wind. The main urban area of Beijing is located south of the research site, and air pollutants in the core urban area may be transported to the research site by wind, which will affect the final observed ozone concentrations. This finding was also confirmed by related studies [68,69]. This is the reason why the direction of wind is also considered in this study.

Table 2. Impact factor interaction detection to ozone concentrations.

Variable	2 m Temperature	10 m U-Wind Component	10 m V-Wind Component	Net Surface Solar Radiation	Surface Pressure	2 m Dewpoint Temperature	RHU *	Solar Altitude	NO ₂
2 m temperature	0.64								
10 m U-wind component	0.66	0.22							
10 m V-wind component	0.67	0.27	0.23						
Net surface solar radiation	0.66	0.39	0.44	0.36					
Surface pressure	0.67	0.30	0.32	0.42	0.27				
2 m dewpoint temperature	0.66	0.29	0.30	0.41	0.33	0.25			
RHU	0.66	0.25	0.25	0.40	0.31	0.30	0.22		
Solar altitude	0.67	0.31	0.38	0.42	0.35	0.34	0.34	0.29	
NO ₂	0.74	0.44	0.46	0.50	0.48	0.45	0.44	0.47	0.41

* Relative humidity: RHU.

To explore the second issue noted in the introduction, we used geodetectors to quantitatively calculate the joint effect of two factors on ozone concentrations on a temporal scale, which is novel compared to previous studies. This study confirms that the temporal application of the wavelet analysis and geographic detectors is feasible.

3.4. General Discussion

Some of our findings are similar to previous studies, while there are also some novel findings in this study. Hourly ozone concentrations are higher in spring and summer and much lower in autumn and winter, with their mean values of 73.33 µg/m³, 97.74 µg/m³, 46.23 µg/m³, and 35.97 µg/m³, respectively (Figure 2a). This result is consistent with previous studies [70–72].

This study analyzes multiscale periods from an oscillating time series, which has not been explored in related studies. There are also fragmented but significant periodic signals, such as 6 h and 12 h in many cases, which indicates that ozone has a smaller periodic signal in addition to the 24 h periodic variations. From the wavelet coherence spectra of NO₂ and O₃, and temperature and O₃, an interesting phenomenon was observed. Regions where NO₂ was in the antiphase with ozone were considerably deficient in regions where temperature and ozone were in phase in 2019. This indicates that in summer and autumn, when temperature is high and NO₂ concentration is low, temperature is the primary factor affecting ozone. In spring and winter, higher NO₂ concentrations control ozone generation when temperature is low. The results of the wavelet analysis indicate that the key factors affecting ozone concentrations differ at different periods within a year, which has not been confirmed by previous studies.

To our knowledge, this is the first time that geodetectors were applied to explore the explanatory power of the individual influencing factors and their interactions on the temporal variations in ozone at an hourly scale. This also provide a new perspective for related research. When discussing the influence of influencing factors on ground-level

ozone concentration, the interaction between factors cannot be ignored, and sometimes it is even very important.

This study also has several limitations. We extracted the periodic properties and phase relationships of ozone and its influencing factors from the oscillatory time series on an hourly scale. One limitation is the uncertainty in the imputation of missing data. This has always been an issue worth exploring for monitoring data; however, it is not the focus of this study. We compared a variety of interpolation methods, and finally concluded that the interpolation method in this study is the most suitable for the ozone time series. The filling of missing data might result in occasional cycles at multiple time scales. Therefore, the analysis in this study only used large contiguous regions in cross wavelet spectrum (XWT) and wavelet coherence spectrum (WTC) to ensure the reliability of the relationship. Other limitations of this study are the length of the time series and the representativeness of the selected station. Because our study focused on an hourly scale, we only selected the time series from the station for 2019. We used a total of 8745 observations, which is sufficient to explore the variations in ozone and its influencing factors during the year. However, this suggests that the relationship between ozone and the influencing factors in this study may be unstable in a longer multiyear term, which is also an interesting issue for future consideration. Furthermore, it should be noted that the findings of this study were concluded from model results only based on one station, which may be different from other stations with different geographical features, such as rural or downtown stations. We will investigate the spatial effects by selecting more types of stations to compare the relationships between influencing factors and ground ozone concentrations in future research.

4. Conclusions

In this work, the time series of ozone and its influencing factors were disentangled and reconstructed to analyze the multiscale relationships with meteorological factors and some precursors using continuous wavelet transform, cross wavelet, and wavelet coherence. Compared with other studies, we quantitatively calculated the period and phase relationships of ozone and its influencing factors. The most significant cycle of ground ozone concentrations was the 22–26 h scale period, and there was a multiscale effect at the scales of 6 h and 12 h. Temperature and ground-level ozone concentrations shared a strong periodic signal, with a positive phase on multiple scales from March to October, while NO₂ and ozone exhibited an antiphase at other times in 2019, indicating that air temperature and NO₂ control ozone production at different times of the year.

We found that the single factor of temperature had the highest power to determine the ground-level ozone concentrations among all the factors. In addition, the interactions between NO₂ and temperature had the strongest explanatory power for the time distribution of ozone concentrations, which has not been found in other studies. The interactions of solar radiation and the southerly wind also has a great impact on the ground ozone concentrations at the research site because densely populated areas are located south of the monitoring site. This finding indicates that the regional transmission of ozone should be considered. Because of the complex and strong multiscale effects of the meteorological factors and precursors on ozone concentrations, the management of ozone pollution should be focused on time scales of ozone pollution and controllable precursors. Long-term mitigation of ozone pollution can be achieved through rational land-use schemes and the control of anthropogenic heat and emission sources. As an emergency response, people can slow the rate of ozone production by using intervention measures such as mist cannon trucks, which can increase humidity and decrease temperature. The findings of this study can help improve the management of urban ozone pollution.

Supplementary Materials: The following supporting information can be downloaded at <https://www.mdpi.com/article/10.3390/atmos14030604/s1>, Figure S1: Z-score normalization time series (a) and wavelet power spectrum (b) of 2 m dew temperature, Figure S2: Z-score normalization time series (a) and wavelet power spectrum (b) of 10 m U component of wind (10 m U wind), Figure S3:

Z-score normalization time series (a) and wavelet power spectrum (b) of relative humidity (RHU), Figure S4: Z-score normalization time series (a) and wavelet power spectrum (b) of solar altitude, Figure S5: Wavelet coherence spectrum (WTC) of 2 m dew temperature and O₃, Figure S6: Crossed wavelet spectrum (XWT) of 2 m dew temperature and O₃, Figure S7: Wavelet coherence spectrum (WTC) of 10 m U component of wind (10 m U wind) and O₃, Figure S8: Crossed wavelet spectrum (XWT) of 10 m U component of wind (10 m U wind) and O₃, Figure S9: Wavelet coherence spectrum (WTC) of 10 m V component of wind (10 m V wind) and O₃, Figure S10: Crossed wavelet spectrum (XWT) of 10 m V component of wind (10 m V wind) and O₃, Figure S11: Wavelet coherence spectrum (WTC) of relative humidity (RHU) and ozone (O₃), Figure S12: Crossed wavelet spectrum (XWT) of relative humidity (RHU) and ozone (O₃), Figure S13: Wavelet coherence spectrum (WTC) of surface net solar radiation (SNSR) and ozone (O₃), Figure S14: Crossed wavelet spectrum (XWT) of surface net solar radiation (SNSR) and ozone (O₃), Figure S15: Wavelet coherence spectrum (WTC) of solar altitude and ozone (O₃), Figure S16: Crossed wavelet spectrum (XWT) of solar altitude and ozone (O₃), Figure S17: Wavelet coherence spectrum (WTC) of surface pressure and ozone (O₃), Figure S18: Crossed wavelet spectrum (XWT) of surface pressure and ozone (O₃), Table S1: Parameters from ERA5 land reanalysis data and observation stations, Table S2: Number and percentage of missing gaps for air pollutants and meteorological data, Table S3: The periods and phase relationship of influencing factors and ozone.

Author Contributions: Conceptualization, J.W. and R.L.; methodology, J.W. and J.D.; validation, R.L., J.D. and J.G.; formal analysis, J.W. and J.G.; resources, P.C.; writing—original draft preparation, J.W. and P.C.; writing—review and editing, R.L. and X.S.; visualization, J.W. and X.S.; supervision, X.Z. and Q.X. All authors have read and agreed to the published version of the manuscript.

Funding: This research was funded by the National Key Research and Development Program of China (Grant No. 2020YFC1807103), the National Natural Science Foundation of China (Grant No. 42341206), Weiqiao-UCAS Special Projects on Low-Carbon Technology (GYY-DTFZ-2022-028), the CAMS Innovation Fund for Medical Sciences (2017-I2M-1-009).

Institutional Review Board Statement: Not applicable.

Informed Consent Statement: Not applicable.

Data Availability Statement: The data presented in this study are available upon request from the corresponding author.

Acknowledgments: Valuable suggestions from Jinfeng Wang in IGSNRR-CAS were greatly appreciated.

Conflicts of Interest: The authors declare no conflict of interest.

References

1. Bower, J.S.; Stevenson, K.J.; Broughton, G.F.J.; Lampert, J.E.; Sweeney, B.P.; Wilken, J. Assessing recent surface ozone concentrations in the U.K. *Atmos. Environ.* **1994**, *28*, 115–128. [[CrossRef](#)]
2. Sheehan, P.; Cheng, E.; English, A.; Sun, F. China's response to the air pollution shock. *Nat. Clim. Chang.* **2014**, *4*, 306–309. [[CrossRef](#)]
3. Wei, W.; Wang, S.; Hao, J.; Cheng, S. Projection of anthropogenic volatile organic compounds (VOCs) emissions in China for the period 2010–2020. *Atmos. Environ.* **2011**, *45*, 6863–6871. [[CrossRef](#)]
4. Zhao, B.; Wang, S.X.; Liu, H.; Xu, J.Y.; Fu, K.; Klimont, Z.; Hao, J.M.; He, K.B.; Cofala, J.; Amann, M. NO_x emissions in China: Historical trends and future perspectives. *Atmos. Chem. Phys.* **2013**, *13*, 9869–9897. [[CrossRef](#)]
5. Wan, W.; Manning, W.J.; Wang, X.; Zhang, H.; Sun, X.; Zhang, Q. Ozone and ozone injury on plants in and around Beijing, China. *Environ. Pollut.* **2014**, *191*, 215–222. [[CrossRef](#)]
6. Verstraeten, W.W.; Neu, J.L.; Williams, J.E.; Bowman, K.W.; Worden, J.R.; Boersma, K.F. Rapid increases in tropospheric ozone production and export from China. *Nat. Geosci.* **2015**, *8*, 690–695. [[CrossRef](#)]
7. Wang, D.; Wei, S.; Luo, H.; Yue, C.; Grunder, O. A novel hybrid model for air quality index forecasting based on two-phase decomposition technique and modified extreme learning machine. *Sci. Total Environ.* **2017**, *580*, 719–733. [[CrossRef](#)]
8. Staehelin, J.; Harris, N.R.P.; Appenzeller, C.; Eberhard, J. Ozone trends: A review. *Rev. Geophys.* **2001**, *39*, 231–290. [[CrossRef](#)]
9. Monks, P.S.; Archibald, A.T.; Colette, A.; Cooper, O.; Coyle, M.; Derwent, R.; Fowler, D.; Granier, C.; Law, K.S.; Mills, G.E.; et al. Tropospheric ozone and its precursors from the urban to the global scale from air quality to short-lived climate forcer. *Atmos. Chem. Phys.* **2015**, *15*, 8889–8973. [[CrossRef](#)]
10. Chen, Z.; Li, R.; Chen, D.; Zhuang, Y.; Gao, B.; Yang, L.; Li, M. Understanding the causal influence of major meteorological factors on ground ozone concentrations across China. *J. Clean. Prod.* **2020**, *242*, 118498. [[CrossRef](#)]

11. Berezina, E.; Moiseenko, K.; Skorokhod, A.; Pankratova, N.V.; Belikov, I.; Belousov, V.; Elansky, N.F. Impact of VOCs and NO_x on ozone formation in Moscow. *Atmosphere* **2020**, *11*, 1262. [[CrossRef](#)]
12. Juráň, S.; Grace, J.; Urban, O. Temporal changes in ozone concentrations and their impact on vegetation. *Atmosphere* **2021**, *12*, 82. [[CrossRef](#)]
13. Luo, G.; Zhang, L.; Hu, X.; Shi, B.; Qiu, R. Assessment of the characteristics and influencing factors of ozone in Fuzhou, China, using wavelet analysis. *Aerosol Air Qual. Res.* **2020**, *20*, 1898–1909. [[CrossRef](#)]
14. Hu, C.; Kang, P.; Jaffe, D.A.; Li, C.; Zhang, X.; Wu, K.; Zhou, M. Understanding the impact of meteorology on ozone in 334 cities of China. *Atmos. Environ.* **2021**, *248*, 118221. [[CrossRef](#)]
15. Li, M.; Yu, S.; Chen, X.; Li, Z.; Zhang, Y.; Wang, L.; Liu, W.; Li, P.; Lichtfouse, E.; Rosenfeld, D.; et al. Large scale control of surface ozone by relative humidity observed during warm seasons in China. *Environ. Chem. Lett.* **2021**, *19*, 3981–3989. [[CrossRef](#)]
16. Gao, M.; Yin, L.; Ning, J. Artificial neural network model for ozone concentration estimation and Monte Carlo analysis. *Atmos. Environ.* **2018**, *184*, 129–139. [[CrossRef](#)]
17. Borhani, F.; Shafiepour Motlagh, M.; Stohl, A.; Rashidi, Y.; Ehsani, A.H. Tropospheric ozone in Tehran, Iran, during the last 20 years. *Environ. Geochem. Health* **2021**, *44*, 3615–3637. [[CrossRef](#)]
18. Vingarzan, R. A review of surface ozone background levels and trends. *Atmos. Environ.* **2004**, *38*, 3431–3442. [[CrossRef](#)]
19. Sousa, S.I.V.; Martins, F.G.; Alvim-Ferraz, M.C.M.; Pereira, M.C. Multiple linear regression and artificial neural networks based on principal components to predict ozone concentrations. *Environ. Modell. Softw.* **2007**, *22*, 97–103. [[CrossRef](#)]
20. Tu, J.; Xia, Z.-G.; Wang, H.; Li, W. Temporal variations in surface ozone and its precursors and meteorological effects at an urban site in China. *Atmos. Res.* **2007**, *85*, 310–337. [[CrossRef](#)]
21. Lu, X.; Hong, J.; Zhang, L.; Cooper, O.R.; Schultz, M.G.; Xu, X.; Wang, T.; Gao, M.; Zhao, Y.; Zhang, Y. Severe surface ozone pollution in China: A global perspective. *Environ. Sci. Technol. Lett.* **2018**, *5*, 487–494. [[CrossRef](#)]
22. Lu, X.; Zhang, L.; Chen, Y.; Zhou, M.; Zheng, B.; Li, K.; Liu, Y.; Lin, J.; Fu, T.M.; Zhang, Q. Exploring 2016–2017 surface ozone pollution over China: Source contributions and meteorological influences. *Atmos. Chem. Phys.* **2019**, *19*, 8339–8361. [[CrossRef](#)]
23. Stafoggia, M.; Johansson, C.; Glantz, P.; Renzi, M.; Shtein, A.; de Hoogh, K.; Kloog, I.; Davoli, M.; Michelozzi, P.; Bellander, T. A random forest approach to estimate daily particulate matter, nitrogen dioxide, and ozone at fine spatial resolution in Sweden. *Atmosphere* **2020**, *11*, 239. [[CrossRef](#)]
24. Li, K.; Chen, L.; Ying, F.; White, S.J.; Jang, C.; Wu, X.; Gao, X.; Hong, S.; Shen, J.; Azzi, M.; et al. Meteorological and chemical impacts on ozone formation: A case study in Hangzhou, China. *Atmos. Res.* **2017**, *196*, 40–52. [[CrossRef](#)]
25. Pu, X.; Wang, T.J.; Huang, X.; Melas, D.; Zanis, P.; Papanastasiou, D.K.; Poupkou, A. Enhanced surface ozone during the heat wave of 2013 in Yangtze River Delta region, China. *Sci. Total Environ.* **2017**, *603–604*, 807–816. [[CrossRef](#)]
26. Chen, Z.; Zhuang, Y.; Xie, X.; Chen, D.; Cheng, N.; Yang, L.; Li, R. Understanding long-term variations of meteorological influences on ground ozone concentrations in Beijing during 2006–2016. *Environ. Pollut.* **2019**, *245*, 29–37. [[CrossRef](#)]
27. Wang, J.; Hu, M.; Zhang, F.; Gao, B. Influential factors detection for surface water quality with geographical detectors in China. *Stoch. Environ. Res. Risk Assess.* **2018**, *32*, 2633–2645. [[CrossRef](#)]
28. Kleanthous, S.; Vrekoussis, M.; Mihalopoulos, N.; Kalabokas, P.; Lelieveld, J. On the temporal and spatial variation of ozone in Cyprus. *Sci. Total Environ.* **2014**, *476–477*, 677–687. [[CrossRef](#)] [[PubMed](#)]
29. Xu, J.; Tie, X.; Gao, W.; Lin, Y.; Fu, Q. Measurement and model analyses of the ozone variation during 2006 to 2015 and its response to emission change in megacity Shanghai, China. *Atmos. Chem. Phys.* **2019**, *19*, 9017–9035. [[CrossRef](#)]
30. Zhao, W.; Fan, S.; Guo, H.; Gao, B.; Sun, J.; Chen, L. Assessing the impact of local meteorological variables on surface ozone in Hong Kong during 2000–2015 using quantile and multiple line regression models. *Atmos. Environ.* **2016**, *144*, 182–193. [[CrossRef](#)]
31. Sharma, A.; Mandal, T.K.; Sharma, S.K.; Shukla, D.K.; Singh, S. Relationships of surface ozone with its precursors, particulate matter and meteorology over Delhi. *J. Atmos. Chem.* **2017**, *74*, 451–474. [[CrossRef](#)]
32. Cheng, N.; Li, R.; Xu, C.; Chen, Z.; Chen, D.; Meng, F.; Cheng, B.; Ma, Z.; Zhuang, Y.; He, B.; et al. Ground ozone variations at an urban and a rural station in Beijing from 2006 to 2017: Trend, meteorological influences and formation regimes. *J. Clean. Prod.* **2019**, *235*, 11–20. [[CrossRef](#)]
33. Kumar, N.; Middey, A.; Rao, P.S. Prediction and examination of seasonal variation of ozone with meteorological parameter through artificial neural network at Neeri, Nagpur, India. *Urban Clim.* **2017**, *20*, 148–167. [[CrossRef](#)]
34. Abdul-Wahab, S.A.; Bakheit, C.S.; Al-Alawi, S.M. Principal component and multiple regression analysis in modelling of ground-level ozone and factors affecting its concentrations. *Environ. Modell. Softw.* **2005**, *20*, 1263–1271. [[CrossRef](#)]
35. So, K.L.; Wang, T. On the local and regional influence on ground-level ozone concentrations in Hong Kong. *Environ. Pollut.* **2003**, *123*, 307–317. [[CrossRef](#)]
36. Bloomfield, P.; Hurd, H.L.; Lund, R.B. Periodic correlation in stratospheric ozone data. *J. Time Ser. Anal.* **1994**, *15*, 127–150. [[CrossRef](#)]
37. Chen, X.; Yin, L.; Fan, Y.; Song, L.; Ji, T.; Liu, Y.; Tian, J.; Zheng, W. Temporal evolution characteristics of PM_{2.5} concentration based on continuous wavelet transform. *Sci. Total Environ.* **2020**, *699*, 134244. [[CrossRef](#)] [[PubMed](#)]
38. Aguilar-Velázquez, D.; Reyes-Ramírez, I. A wavelet analysis of multiday extreme ozone and its precursors in Mexico city during 2015–2016. *Atmos. Environ.* **2018**, *188*, 112–119. [[CrossRef](#)]
39. Tian, J.; Fang, C.; Qiu, J.; Wang, J. Analysis of ozone pollution characteristics and influencing factors in northeast economic cooperation region, China. *Atmosphere* **2021**, *12*, 843. [[CrossRef](#)]

40. Al Yammahi, A.; Aung, Z. A study of nitrogen dioxide (NO₂) periodicity over the United Arab Emirates using wavelet analysis. *Sci. Rep.* **2022**, *12*, 18144. [[CrossRef](#)] [[PubMed](#)]
41. Chen, Y.; Li, H.; Karimian, H.; Li, M.; Fan, Q.; Xu, Z. Spatio-temporal variation of ozone pollution risk and its influencing factors in China based on geodetector and geospatial models. *Chemosphere* **2022**, *302*, 134843. [[CrossRef](#)]
42. Chen, Y.; Zhou, Y.; NixiaCiren; Zhang, H.; Wang, C.; GesangDeji; Wang, X. Spatiotemporal variations of surface ozone and its influencing factors across Tibet: A geodetector-based study. *Sci. Total Environ.* **2022**, *813*, 152651. [[CrossRef](#)] [[PubMed](#)]
43. Liu, P.; Song, H.; Wang, T.; Wang, F.; Li, X.; Miao, C.; Zhao, H. Effects of meteorological conditions and anthropogenic precursors on ground-level ozone concentrations in Chinese cities. *Environ. Pollut.* **2020**, *262*, 114366. [[CrossRef](#)] [[PubMed](#)]
44. Wang, Z.-b.; Li, J.-x.; Liang, L.-w. Spatio-temporal evolution of ozone pollution and its influencing factors in the Teijing-Tianjin-Hebei urban agglomeration. *Environ. Pollut.* **2020**, *256*, 113419. [[CrossRef](#)] [[PubMed](#)]
45. Tan, X.; Qian, Y.; Wang, H.; Fu, J.; Wu, J. Analysis of the spatial and temporal patterns of ground-level ozone concentrations in the Guangdong–Hong Kong–Macao greater bay area and the contribution of influencing factors. *Remote Sens.* **2022**, *14*, 5796. [[CrossRef](#)]
46. Haagen-Smit, A.J.; Bradley, C.E.; Fox, M.M. Ozone formation in photochemical oxidation of organic substances. *Ind. Eng. Chem.* **1953**, *45*, 2086–2089. [[CrossRef](#)]
47. Bai, L.; Jiang, L.; Yang, D.-y.; Liu, Y.-b. Quantifying the spatial heterogeneity influences of natural and socioeconomic factors and their interactions on air pollution using the geographical detector method: A case study of the Yangtze River Economic Belt, China. *J. Clean. Prod.* **2019**, *232*, 692–704. [[CrossRef](#)]
48. Jing, P.; O'Brien, T.; Streets, D.G.; Patel, M. Relationship of ground-level ozone with synoptic weather conditions in Chicago. *Urban Clim.* **2016**, *17*, 161–175. [[CrossRef](#)]
49. Hersbach, H.; Bell, B.; Berrisford, P.; Hirahara, S.; Horányi, A.; Muñoz-Sabater, J.; Nicolas, J.; Peubey, C.; Radu, R.; Schepers, D.; et al. The ERA5 global reanalysis. *Q. J. R. Meteorol. Soc.* **2020**, *146*, 1999–2049. [[CrossRef](#)]
50. Torrence, C.; Compo, G.P. A practical guide to wavelet analysis. *Bull. Am. Meteorol. Soc.* **1998**, *79*, 61–78. [[CrossRef](#)]
51. Ji, Q.; Xu, F.; Zhang, Y. Study on ENSO time-frequency characteristics in recent 50 years and its correlation with typhoon in the South China Sea. *J. Guangdong Ocean Univ.* **2018**, *38*, 71–79. [[CrossRef](#)]
52. Grinsted, A.; Moore, J.C.; Jevrejeva, S. Application of the cross wavelet transform and wavelet coherence to geophysical time series. *Nonlin. Process. Geophys.* **2004**, *11*, 561–566. [[CrossRef](#)]
53. Sun, W.; Cheng, B. Application of cross wavelet transformation to analysis on regional climate variations. *J. Appl. Meteor. Sci.* **2008**, *19*, 479–487. (In Chinese) [[CrossRef](#)]
54. Wang, J.-F.; Zhang, T.-L.; Fu, B.-J. A measure of spatial stratified heterogeneity. *Ecol. Indic.* **2016**, *67*, 250–256. [[CrossRef](#)]
55. Wang, J.F.; Li, X.H.; Christakos, G.; Liao, Y.L.; Zhang, T.; Gu, X.; Zheng, X.Y. Geographical detectors-based health risk assessment and its application in the neural tube defects study of the Heshun region, China. *Int. J. Geog. Inf. Sci.* **2010**, *24*, 107–127. [[CrossRef](#)]
56. Lu, K.; Zhang, Y.; Su, H.; Shao, M.; Zeng, L.; Zhong, L.; Xiang, Y.; Chang, C.; Chou, C.K.C.; Wahner, A. Regional ozone pollution and key controlling factors of photochemical ozone production in Pearl River Delta during summer time. *Sci. China Chem.* **2010**, *53*, 651–663. [[CrossRef](#)]
57. Ma, M.; Yao, G.; Guo, J.; Bai, K. Distinct spatiotemporal variation patterns of surface ozone in China due to diverse influential factors. *J. Environ. Manag.* **2021**, *288*, 112368. [[CrossRef](#)]
58. Coates, J.; Mar, K.A.; Ojha, N.; Butler, T.M. The influence of temperature on ozone production under varying NO_x conditions—A modelling study. *Atmos. Chem. Phys.* **2016**, *16*, 11601–11615. [[CrossRef](#)]
59. Stathopoulou, E.; Mihalakakou, G.; Santamouris, M.; Bagiorgas, H.S. On the impact of temperature on tropospheric ozone concentration levels in urban environments. *J. Earth Syst. Sci.* **2008**, *117*, 227–236. [[CrossRef](#)]
60. Ninneman, M.; Jaffe, D. Observed relationship between ozone and temperature for urban nonattainment areas in the United States. *Atmosphere* **2021**, *12*, 1235. [[CrossRef](#)]
61. Kinosian, J.R. Ozone-precursor relationships from EKMA diagrams. *Environ. Sci. Technol.* **1982**, *16*, 880–883. [[CrossRef](#)] [[PubMed](#)]
62. Bloomer, B.J.; Stehr, J.W.; Piety, C.A.; Salawitch, R.J.; Dickerson, R.R. Observed relationships of ozone air pollution with temperature and emissions. *Geophys. Res. Lett.* **2009**, *36*, L09803. [[CrossRef](#)]
63. Atkinson, R. Atmospheric chemistry of VOCs and NO_x. *Atmos. Environ.* **2000**, *34*, 2063–2101. [[CrossRef](#)]
64. Jacob, D.J. Heterogeneous chemistry and tropospheric ozone. *Atmos. Environ.* **2000**, *34*, 2131–2159. [[CrossRef](#)]
65. Fowler, D.; Amann, M.; Anderson, R.; Ashmore, M.; Cox, P.; Depledge, M.; Derwent, D.; Grennfelt, P.; Hewitt, N.; Hov, O. *Ground-Level Ozone in the 21st Century: Future Trends, Impacts and Policy Implications*; The Royal Society: London, UK, 2008.
66. He, J.; Pan, Z.; Liu, D.; Guo, X. Exploring the regional differences of ecosystem health and its driving factors in China. *Sci. Total Environ.* **2019**, *673*, 553–564. [[CrossRef](#)]
67. Han, S.; Bian, H.; Feng, Y.; Liu, A.; Li, X.; Zeng, F.; Zhang, X. Analysis of the relationship between O₃, NO and NO₂ in Tianjin, China. *Aerosol Air Qual. Res.* **2011**, *11*, 128–139. [[CrossRef](#)]
68. Xu, J.; Zhang, X.; Zhao, X.; Xu, X.; Meng, W. Influence of summer local circulation on ozone transport in downwind areas of Beijing. *China Environ. Sci. Chin. Ed.* **2009**, *29*, 1140–1146. [[CrossRef](#)]
69. Li, Y. Observation-Based Analysis of Causes and Sources of Ambient Air Ozone Pollution in Beijing. Ph.D. Thesis, Shan Dong University, Jinan, China, 2021. [[CrossRef](#)]

70. Liu, R.; Ma, Z.; Liu, Y.; Shao, Y.; Zhao, W.; Bi, J. Spatiotemporal distributions of surface ozone levels in China from 2005 to 2017: A machine learning approach. *Environ. Int.* **2020**, *142*, 105823. [[CrossRef](#)]
71. Wang, Y.; Wild, O.; Chen, X.; Wu, Q.; Gao, M.; Chen, H.; Qi, Y.; Wang, Z. Health impacts of long-term ozone exposure in China over 2013–2017. *Environ. Int.* **2020**, *144*, 106030. [[CrossRef](#)]
72. Maji, K.J.; Ye, W.-F.; Arora, M.; Nagendra, S.M.S. Ozone pollution in Chinese cities: Assessment of seasonal variation, health effects and economic burden. *Environ. Pollut.* **2019**, *247*, 792–801. [[CrossRef](#)]

Disclaimer/Publisher’s Note: The statements, opinions and data contained in all publications are solely those of the individual author(s) and contributor(s) and not of MDPI and/or the editor(s). MDPI and/or the editor(s) disclaim responsibility for any injury to people or property resulting from any ideas, methods, instructions or products referred to in the content.